Superconductivity and strong intrinsic defects in $LaPd_{1-x}Bi_2$

Fei Han,[1] Christos D. Malliakas,[1,2] Constantinos C. Stoumpos,[1] Mihai Sturza,[1] Helmut Claus,[1] Duck Young Chung,[1] and Mercouri G. Kanatzidis[1,2,*]

[1]*Materials Science Division, Argonne National Laboratory, Argonne, Illinois 60439, United States*

[2]*Department of Chemistry, Northwestern University, Evanston, Illinois 60208, United States*

(Received 26 August 2013; revised manuscript received 10 October 2013; published 22 October 2013)

Two new phases $LaPd_{1-x}Bi_2$ and $CePd_{1-x}Bi_2$ were obtained by growing single crystals in Bi flux. They adopt the tetragonal $ZrCuSi_2$-type structure and feature Bi-square nets and PbO-type PdBi layers with significant partial Pd occupancy. Bulk superconductivity at 2.1 K and metallic behavior above T_c are observed in $LaPd_{1-x}Bi_2$. A small residual resistance ratio (RRR) indicates a strong scattering effect induced by the Pd vacancies, which implies an *s*-wave pairing symmetry in $LaPd_{1-x}Bi_2$. The broadening of the resistivity transition was measured under different magnetic fields demonstrating a high upper critical field of 3 T. Hall effect measurements reveal dominantly electron-like charge carriers and single-band transport behavior in $LaPd_{1-x}Bi_2$. The paramagnetic $CePd_{1-x}Bi_2$ is nonsuperconducting but shows antiferromagnetic ordering below 6 K.

DOI: 10.1103/PhysRevB.88.144511 PACS number(s): 74.70.−b, 74.62.Dh, 74.25.Jb

I. INTRODUCTION

The discovery of the iron-based superconductors with unconventional superconductivity has attracted great attention and triggered extensive research in the fields of condensed matter physics and materials science.[1] The family of the iron-based superconductors has been greatly expanded to several families such as the so-called 1111 phase (*Ln*FeAsO, *Ae*FeAsF, *Ln* = rare earth elements, *Ae* = alkaline earth elements),[1–4] 122 phase ($AeFe_2As_2$, *Ae* = alkaline earth elements),[5,6] 111 phase (LiFeAs, NaFeAs) (Refs. 7–9), and 11 phase (FeSe) (Ref. 10), 3442 phase ($La_3Ni_4P_4O_2$) (Ref. 11), 21311 phase (Sr_2ScO_3FeP, Sr_2VO_3FeAs) (Ref. 12 and 13), $A_xFe_{2-y}Se_2$ phase (*A* = alkaline elements),[14] and so on. Among these, the common Fe*X* (*X* = pnictogen or chalcogen) layers are responsible for the superconductivity. Superconductivity was also observed in compounds with iron completely substituted by other 3*d*, 4*d*, or 5*d* transition metals.[15–21] After several 3*d*, 4*d*, 5*d* transition metal-phosphide, arsenide, germanide, or chalcogenide superconductors were discovered, attention has now focused on bismuthides and related systems.

Recently, polycrystalline $CeNi_{1-x}Bi_2$ was reported to be superconducting at 4.2 K (Ref. 22), and the authors argued that the light electron coming from the Bi square net is responsible for the superconductivity while the heavy electron from the $Ni_{1-x}Bi$ layer is responsible for the strong interaction with Ce $4f$ which yields the antiferromagnetic (AFM) transition. However, the results obtained on single crystals by another group were quite different.[23] Superconductivity was found only in the single crystals of $LaNi_{1-x}Bi_2$, whereas in single crystals of $RNi_{1-x}Bi_2$ (*R* = Ce-Nd, Sm, Gd-Dy) superconductivity was absent while local-moment-like behavior and AFM order were observed at low temperatures.

Here we report the magnetic, transport properties, and electronic structure calculations of $LaPd_{1-x}Bi_2$ and $CePd_{1-x}Bi_2$, which exhibit strong vacancy defects in the square Pd sublattice. $LaPd_{1-x}Bi_2$ is found to be superconducting at 2.1 K while $CePd_{1-x}Bi_2$ has an AFM transition at 6 K.

II. EXPERIMENTAL DETAILS

Single-crystalline $LaPd_{1-x}Bi_2$ and $CePd_{1-x}Bi_2$ were grown using a self-flux method, similar to a previous synthesis of Ce*T*Bi_2 (*T* = Ni, Cu, Ag) (Ref. 24). The starting materials La/Ce, Pd, and Bi with mole ratio of 1 : 1 : 12 and total mass of 3 grams were weighed, mixed, and placed in an alumina crucible. All handling was performed in a glove box with a protective argon atmosphere (both H_2O and O_2 are limited below 0.1 ppm). Then the alumina crucible was jacketed by an evacuated silica tube. The tube was heated to 900° C in a box furnace and kept at 900° C for 10 hours. A slow-cooling process from 900° to 500° C was carried out and at 500° C the excess Bi flux was removed by centrifugation. The obtained crystals were shiny silver-color plates with a typical dimension of 5 × 5 × 0.5 mm.

A single-crystal x-ray diffraction (SCXRD) measurement was carried out on a STOE diffractometer. Data reducing was performed with the software X-AREA, and the structure was solved by direct methods using the SHELXTL software.[25]

Powder x-ray diffraction (PXRD) data were collected on a PANalytical diffractometer with θ-2θ scan at room temperature and analyzed by the Rietveld method with the GSAS software.[26]

The magnetic susceptibility data for $LaPd_{1-x}Bi_2$ were collected on a home-built superconducting quantum interference device (SQUID) while those for $CePd_{1-x}Bi_2$ were collected with the AC/DC Magnetometry System (ACMS) option on the Quantum Design physical property measurement system (PPMS).

Transport properties measurements including resistivity and the Hall effect were simultaneously performed with a standard six-probe method on the Quantum Design physical property measurement system (PPMS).

III. RESULTS AND DISCUSSION

A. Crystal structure

Figure 1(a) shows the plate-like crystal habit of $LaPd_{1-x}Bi_2$ and $CePd_{1-x}Bi_2$ crystals obtained. Both $LaPd_{1-x}Bi_2$ and

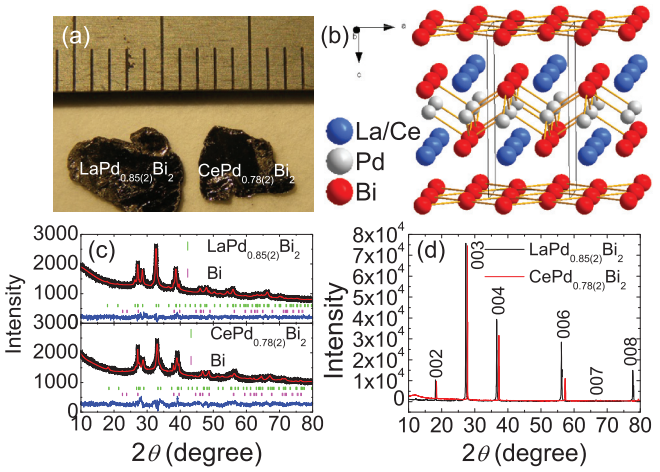

FIG. 1. (Color online) (a) Photograph of $LaPd_{0.85(2)}Bi_2$ and $CePd_{0.78(2)}Bi_2$ crystals. (b) Crystal structure of $LaPd_{0.85(2)}Bi_2$ and $CePd_{0.78(2)}Bi_2$. (c) Powder x-ray diffraction patterns and Rietveld refinements for $LaPd_{0.85(2)}Bi_2$ and $CePd_{0.78(2)}Bi_2$. (d) $00l$ reflections on the fresh-cleaved surfaces of $LaPd_{0.85(2)}Bi_2$ and $CePd_{0.78(2)}Bi_2$ crystals.

$CePd_{1-x}Bi_2$ adopt the tetragonal $ZrCuSi_2$-type structure and feature partial occupancy of Pd atoms as determined by single crystal x-ray diffraction, Fig. 1(b). The compositions are $LaPd_{0.85(2)}Bi_2$ and $CePd_{0.78(2)}Bi_2$. The resulting structure parameters are listed in Table I.

In the structure, the $Pd_{1-x}Bi$ layers adopt the same PbO-type structure as the FeAs layers, while the additional Bi atoms at the other kind of anionic sites form an extended Bi square net. We sparingly raise the possibility of charge density wave (CDW) in the Bi square net since CDW is frequently observed in anionic square nets (e.g., Te or Ga square net).[27–32] Electronic calculations (to be discussed later) on stoichiometric $LaPdBi_2$ indicate the possibility of Fermi surface nesting which is important for CDW formation.[33–35]

The room-temperature PXRD patterns and the Rietveld refinements for the ground samples of $LaPd_{0.85(2)}Bi_2$ and $CePd_{0.78(2)}Bi_2$ are shown in Fig. 1(c). We found the crystals are malleable during grinding which makes the hk containing Bragg peaks broad. Figure 1(d) presents the $00l$ reflections on the fresh-cleaved surfaces of crystals, which indicates the surfaces of the $LaPd_{0.85(2)}Bi_2$ and $CePd_{0.78(2)}Bi_2$ crystals correspond to the ab plane. All transport properties discussed later were measured with the electric current parallel to the ab plane and the field perpendicular to the ab plane. The $00l$ peaks are very sharp, indicating excellent crystalline quality. The slight peak shift towards higher Bragg angles in the case of $CePd_{0.78(2)}Bi_2$ is due to the lanthanide contraction rule.

TABLE I. Crystal data and structure refinement for $LaPd_{1-x}Bi_2$ and $CePd_{1-x}Bi_2$.

Empirical formula	$LaPd_{0.85(2)}Bi_2$	$CePd_{0.78(2)}Bi_2$
Formula weight	647.31	641.07
Temperature	293(2) K	293(2) K
Crystal system	Tetragonal	Tetragonal
Space group	$P4/nmm$	$P4/nmm$
Unit cell dimensions	$a = 4.6340(5)$ Å, $\alpha = 90^\circ$	$a = 4.6136(19)$ Å, $\alpha = 90^\circ$
	$b = 4.6340(5)$ Å, $\beta = 90^\circ$	$b = 4.6136(19)$ Å, $\beta = 90^\circ$
	$c = 9.9436(17)$ Å, $\gamma = 90^\circ$	$a = 9.650(6)$ Å, $\gamma = 90^\circ$
Volume	213.53(5) Å^3	205.39(17) Å^3
Z	2	2
Density (calculated)	10.068 g/cm^3	10.366 g/cm^3
Absorption coefficient	95.262 mm^{-1}	99.419 mm^{-1}
F(000)	524	520
Reflections collected	871	609
Independent reflections	140 [$R_{int} = 0.0657$]	134 [$R_{int} = 0.1016$]
Completeness to $\theta = 24.96/24.92^\circ$	100%	97.8%
Refinement method	Full-matrix least squares on F^2	Full-matrix least squares on F^2
Data/restraints/parameters	140/0/12	134/0/12
Goodness-of-fit	1.001	1.031
Final R indices [$>2\sigma$(I)]	$R_{obs} = 0.0273$, $wR_{obs} = 0.0775$	$R_{obs} = 0.0388$, $wR_{obs} = 0.0579$
R indices [all data]	$R_{all} = 0.0328$, $wR_{all} = 0.1005$	$R_{all} = 0.0538$, $wR_{all} = 0.0602$
Atomic coordinates:		
La/Ce	$2c\left[\frac{1}{4}, \frac{1}{4}, 0.2623(3)\right]$	$2c\left[\frac{1}{4}, \frac{1}{4}, 0.2687(3)\right]$
	Occupancy = 1, $U_{eq} = 0.0017(1)$	Occupancy = 1, $U_{eq} = 0.0013(1)$
Pd	$2b\left[\frac{3}{4}, \frac{1}{4}, \frac{1}{2}\right]$	$2b\left[\frac{3}{4}, \frac{1}{4}, \frac{1}{2}\right]$
	Occupancy = 0.85(2), $U_{eq} = 0.0018(2)$	Occupancy = 0.78(2), $U_{eq} = 0.0014(2)$
Bi	$2a\left[\frac{3}{4}, \frac{1}{4}, 0\right]$	$2a\left[\frac{3}{4}, \frac{1}{4}, 0\right]$
	Occupancy = 1, $U_{eq} = 0.0017(1)$	Occupancy = 1, $U_{eq} = 0.0015(1)$
Bi	$2c\left[\frac{1}{4}, \frac{1}{4}, 0.6637(2)\right]$	$2c\left[\frac{1}{4}, \frac{1}{4}, 0.6593(2)\right]$
	Occupancy = 1, $U_{eq} = 0.0024(1)$	Occupancy = 1, $U_{eq} = 0.0018(1)$

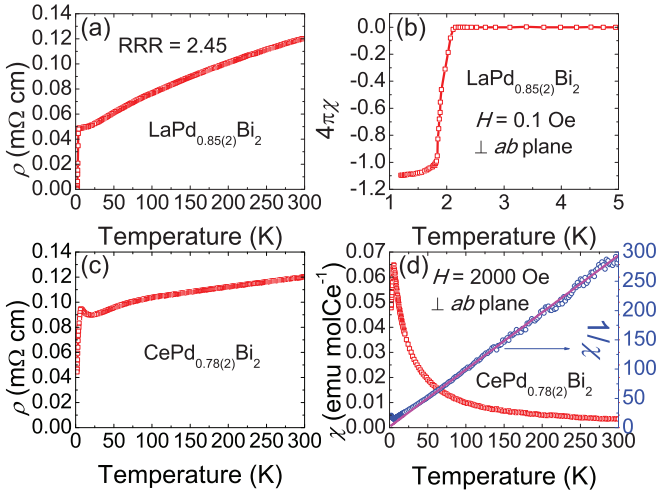

FIG. 2. (Color online) (a) In-plane resistivity measured on a single-crystal $LaPd_{0.85(2)}Bi_2$ sample. (b) Diamagnetic shield below 2.1 K for the same $LaPd_{0.85(2)}Bi_2$ sample. (c) In-plane resistivity measured on a single-crystal $CePd_{0.78(2)}Bi_2$ sample. (d) Temperature dependence of magnetic susceptibility $\chi(T)$ and its inverse $1/\chi$ for $CePd_{0.78(2)}Bi_2$ measured with the field perpendicular to the ab plane.

B. Resistivity and magnetic susceptibility

The temperature dependence of resistivity for $LaPd_{0.85(2)}Bi_2$ is plotted in Fig. 2(a). A superconducting transition occurs at around 2 K (zero-resistivity point), and the transition is displayed more precisely in Fig. 3 with the temperature region from 0 to 10 K. Metallic behavior exists in the normal state: The resistivity shows a linear relationship with the temperature above 30 K and levels off to a constant value (the so-called residual resistivity) below 30 K. Dividing the resistivity at 300 K by the resistivity at T_c(onset), we can get the residual resistance ratio (RRR) of 2.45. The relatively small RRR indicates a strong scattering effect in the conductive layers. Considering the partial Pd occupancy in the lattice, we think the strong electron scattering is brought by the Pd vacancies in the $Pd_{1-x}Bi$ layers. The Pd vacancies can be thought of as nonmagnetic impurities and play the role of scattering centers. In a conventional superconductor with s-wave pairing symmetry, the nonmagnetic impurities will not lead to an apparent pair-breaking effect, therefore no quasiparticle density of states (DOS) can be generated at the Fermi energy. This was called Anderson's theorem.[36] In sharp contrast, in a d-wave superconductor, nonmagnetic impurities can induce a high DOS due to the existence of nodes. Based on this point, the superconductivity in $LaPd_{0.85(2)}Bi_2$ is likely s wave. However, more work will be required to further explore this point. In Fig. 2(b), we present the temperature dependence of magnetic susceptibility showing the demagnetization effect. A full diamagnetic shield is achieved below 2.1 K which corresponds to the zero-resistivity point mentioned above. So, below 2.1 K the superconductivity is bulk, and above 2.1 K superconducting fluctuation or sample inhomogeneity may account for the transition width in the resistivity.

The temperature dependence of resistivity for $CePd_{0.78(2)}Bi_2$ is also displayed in Fig. 2(c) for comparison. Above 75 K, the in-plane resistivity shows a linear behavior and weak temperature dependence, similar to $LaPd_{0.85(2)}Bi_2$. However, a sharp peak corresponding to the AFM transition is observed at 6 K. The temperature dependence of molar magnetic susceptibility $\chi(T)$ and its inverse $1/\chi$ for $CePd_{0.78(2)}Bi_2$ measured in a field of 0.2 T is shown in Fig. 2(d). The AFM ordering of the Ce moments below 6 K is confirmed by the peak at 6 K in $\chi(T)$, and the high-temperature susceptibility obeys the simple Curie-Weiss law $\chi = C/(T\text{-}\Theta_P)$. From the fitting process with the Curie-Weiss law, a paramagnetic Curie temperature of $\Theta_P = -1.5$ K and an effective magnetic moment of $\mu_{\rm eff} = 2.86\ \mu_B$/Ce are obtained. The negative Θ_P suggests a tendency toward antiferromagnetic correlation between the Ce moments at high temperatures. The value of $\mu_{\rm eff}$ is very close to that of $CeNiBi_2$ (Ref. 37) and comparable to the expected value for a free Ce^{3+} ion (2.54 μ_B/Ce), which indicates that the magnetic moments of Ce are well localized in the compound.

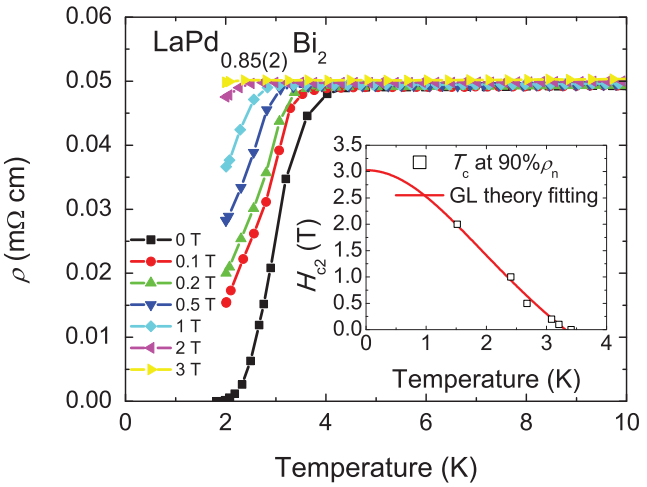

FIG. 3. (Color online) Temperature dependence of in-plane resistivity for $LaPd_{0.85(2)}Bi_2$ at various magnetic fields which are perpendicular to the ab plane. The inset shows the upper critical fields as a function of temperature. The red solid line indicates the theoretical fitting based on the Ginzburg-Landau theory.

C. Upper critical field

To obtain the upper critical field for $LaPd_{0.85(2)}Bi_2$, we carried out the resistivity measurements at different applied magnetic fields. The original data are plotted in the main frame of Fig. 3. We use the criterion of $90\%\rho_n$ to estimate the upper critical field based on the Ginzburg-Landau (GL) theory,[38] as shown in the inset of Fig. 3. The following equation has been extracted from the GL theory: $H_{c2}(T) = H_{c2}(0) \times (1-t^2)/(1+t^2)$, where $t = T/T_c$ is the reduced temperature and $H_{c2}(0)$ is the upper critical field at zero temperature. The measured data in the inset of Fig. 3 were well fitted using the equation above (red solid line). The zero-temperature upper critical field was determined to be 3 T from the fit. This $H_{c2}(0)$ value is quite large relative to the low T_c, so we conclude $LaPd_{0.85(2)}Bi_2$ is a type-II superconductor.

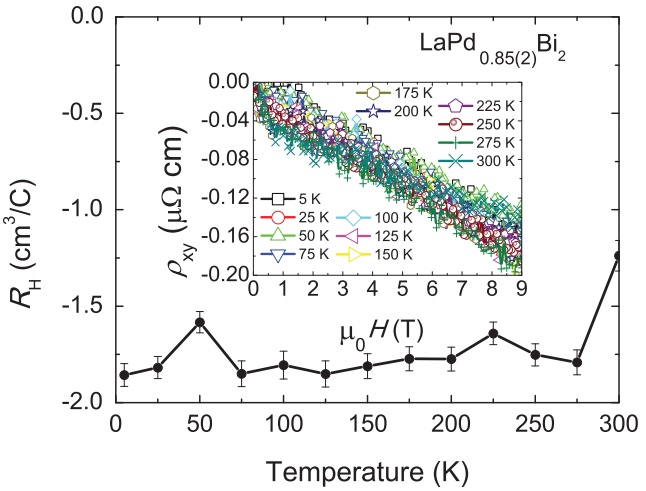

FIG. 4. (Color online) Temperature dependence of Hall coefficient R_H (with error bars) for $LaPd_{0.85(2)}Bi_2$ measured with the field perpendicular to the ab plane. Inset: Hall resistivity ρ_{xy} versus magnetic field $\mu_0 H$ at different temperatures.

D. Hall effect

To get a deeper understanding of the conducting carriers in the $LaPd_{0.85(2)}Bi_2$ phase, we measured the Hall effect. The inset of Fig. 4 shows the magnetic-field dependence of Hall resistivity ρ_{xy} at different temperatures. In the experiment, ρ_{xy} was taken as $\rho_{xy} = [\rho(+H) - \rho(-H)]/2$ at each point to eliminate the effect of the possible misalignment of Hall electrodes. The temperature dependence of the Hall coefficient R_H is plotted in the main frame of Fig. 4. The Hall coefficient R_H is negative and nearly constant over the whole temperature range. The negative sign of R_H shows that electron-type charge carriers dominate the charge transport. Taking the average value of $R_H = 1.7 \times 10^{-4}$ cm^3/C into the equation $R_H = 1/ne$, we can get the electron concentration $n = 3.7 \times 10^{22}$ /cm^3. That the R_H is almost independent of temperature indicates largely a single-band character. This view needs to be confirmed by temperature-dependent angle resolved photoemission spectroscopy (ARPES).

IV. BAND STRUCTURE CALCULATIONS

Electronic structure calculations were performed on the stoichiometric $LaPdBi_2$ model using the self-consistent full-potential linearized augmented plane wave method (LAPW)[39] within density functional theory (DFT),[40,41] using the generalized gradient approximation (GGA) of Perdew, Burke, and Ernzerhof[42] for the exchange and correlation potential. The values of the atomic radii were taken to be 2.6 a.u. for all atoms where a.u. is the atomic unit (0.529 Å). The convergence of the self-consistent iterations was performed for 630 k points inside the irreducible Brillouin zone to within 0.0001 Ry with a cutoff of -6.0 Ry between the valence and the core states. Scalar relativistic corrections were included and a spin-orbit interaction was incorporated using a second variational procedure.[43] The calculations were performed using the WIEN2K program.[44]

Band structure calculations at the DFT level confirmed the metallic character of the $LaPd_{1-x}Bi_2$ system, as shown in Fig. 5. In the fully stoichiometric $LaPdBi_2$, bands near the Fermi level are dispersive (see Fig. 6) where La, Bi(1) (in the PbO-type layer), and Bi(2) (in the square net) bands have almost equal contribution at the Fermi level. Pd bands on the other hand dominate at the Fermi level with almost double the contribution with respect to the other atoms.

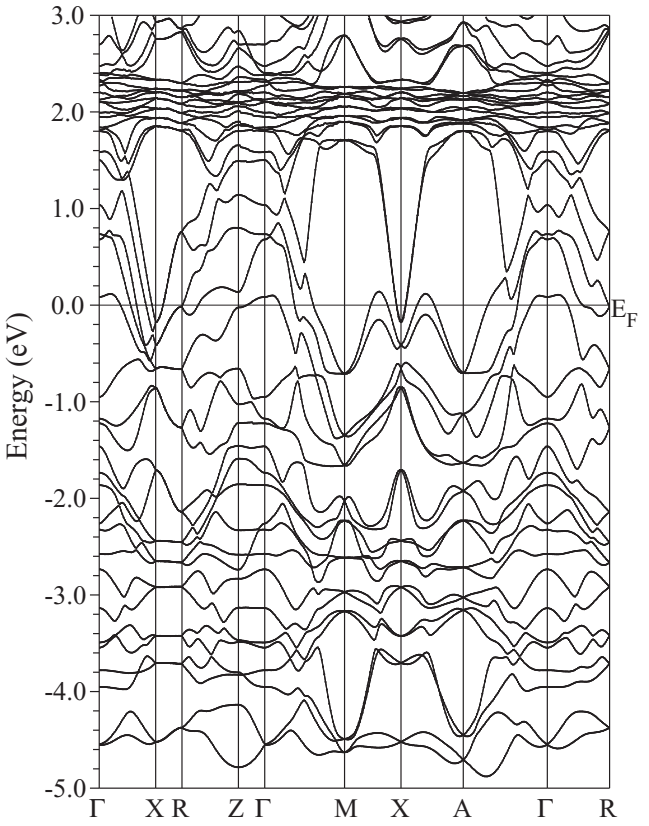

FIG. 5. Calculated band structure near the Fermi level for stoichiometric $LaPdBi_2$.

Consequently, any change in the concentration of Pd atoms in $LaPd_{1-x}Bi_2$ will strongly affect the Fermi surface, as shown in Fig. 7. The number of bands crossing the Fermi level varies with x value. In more detail: There are ten bands crossing the Fermi energy for $x = 0$, six bands for $x = 0.043$, six bands for $x = 0.065$, four bands for $x = 0.108$, six bands for $x = 0.130$, and eight bands for $x = 0.150$. Band structure

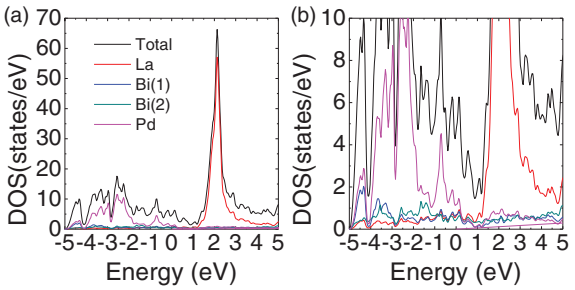

FIG. 6. (Color online) (a) Density of states (DOS) plot near the Fermi level for the fully stoichiometric $LaPdBi_2$. La, Bi, and Pd bands have almost the same contribution at the Fermi level. (b) Enlarged DOS plot showing the dominant contribution of Pd bands near the Fermi level.

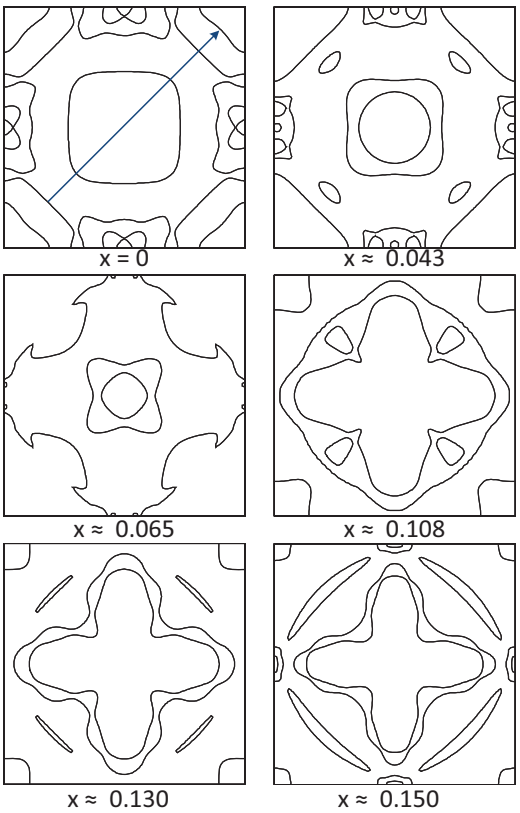

FIG. 7. (Color online) Changes in the topology of the Fermi surface as a function of concentration of Pd vacancies in $LaPd_{1-x}Bi_2$. The potential for nesting seems to be more prominent in the fully stoichiometric case ($x = 0$).

calculations support the possibility of Fermi surface nesting near the fully stoichiometric case in $LaPd_{1-x}Bi_2$. By creating Pd vacancies the Fermi surface nesting is avoided which suppresses any potential CDW on the Bi net. Such kinds of suppression of a putative CDW may drive the $LaPd_{1-x}Bi_2$ system to superconductivity. The electronic structure and Fermi surface topology of $LaPdBi_2$ is quite different from those in $SrMnBi_2$ (Ref. 45), a related compound which also has a Bi net but crystallizes in a different space group. In the later, Bi states dominate at the Fermi level where a more equitable contribution from all atoms at the Fermi level is suggested in $LaPdBi_2$.

V. CONCLUSION

Bulk superconductivity at 2.1 K was discovered in $LaPd_{1-x}Bi_2$ while $CePd_{1-x}Bi_2$ has an AFM transition at 6 K. The partial Pd occupancy determined by single crystal x-ray diffraction leads to a strong scattering effect in the conductive layers of $LaPd_{1-x}Bi_2$ and $CePd_{1-x}Bi_2$. According to Anderson's theorem,[36] the strong scattering effect implies the superconductivity in $LaPd_{1-x}Bi_2$ is s-wave symmetric. The upper critical field of 3 T strongly recommends $LaPd_{1-x}Bi_2$ is a type-II superconductor. The temperature independence of the Hall coefficient may suggest a single-band dominates the transport in $LaPd_{1-x}Bi_2$. On the other hand, the absence of superconductivity and the appearance of AFM order below 6 K in $CePd_{1-x}Bi_2$ jointly suggest the superconductivity and magnetism are not able to coexist. The $RPd_{1-x}Bi_2$ system (R = La, Ce) and the iron-based superconductors have not only similarities but also differences. (1) The iron-based superconductors have the so-called $s\pm$ state with the pairing symmetry being s wave but a sign change occurring between different bands.[46,47] Similarly, our $LaPd_{1-x}Bi_2$ is also likely s-wave symmetric. (2) By contrast the f-d hybridization in $CePd_{1-x}Bi_2$ quenches the superconductivity as, for example, in CeOFeP and $EuFe_{2-x}Co_xAs_2$ (Refs. 48 and 49). (3) In the iron-based superconductors the interplay of magnetism and superconductivity widely exists,[50] but in $LaPd_{1-x}Bi_2$ no magnetism is found. (4) In the iron-based superconductors the interband scattering of electrons induced by spin fluctuation plays an important role in the origin of superconductivity,[51–53] but in $LaPd_{1-x}Bi_2$ no such interband scattering is present since single-band dominates its transport. Instead, the Pd orbital contribution is dominant at the Fermi level, which, coupled with Pd vacancies, may be important for superconductivity. Considering the different features between $LaPd_{1-x}Bi_2$ and iron-based superconductors, we suggest that $LaPd_{1-x}Bi_2$ have a differing electron phonon coupling mechanism than the one in iron-based superconductors.

ACKNOWLEDGMENT

This work is supported by the US Department of Energy, Office of Basic Energy Sciences under Contract No. DE-AC02-06CH11357.

*m-kanatzidis@northwestern.edu

[1] Y. Kamihara, T. Watanabe, M. Hirano, and H. Hosono, J. Am. Chem. Soc. **130**, 3296 (2008).
[2] S. Matsuishi, Y. Inoue, T. Nomura, H. Yanagi, M. Hirano, and H. Hosono, J. Am. Chem. Soc. **130**, 14428 (2008).
[3] F. Han, X. Zhu, G. Mu, P. Cheng, and H. H. Wen, Phys. Rev. B **78**, 180503(R) (2008).
[4] M. Tegel, S. Johansson, V. Weiss, I. Schellenberg, W. Hermes, R. Pottgen, and D. Johrendt, Europhys. Lett. **84**, 67007 (2008).
[5] M. Rotter, M. Tegel, and D. Johrendt, Phys. Rev. Lett. **101**, 107006 (2008).
[6] K. Sasmal, B. Lv, B. Lorenz, A. M. Guloy, F. Chen, Y. Y. Xue, and C. W. Chu, Phys. Rev. Lett. **101**, 107007 (2008).
[7] X. C. Wang, Q. Q. Liu, Y. X. Lv, W. B. Gao, L. X. Yang, R. C. Yu, F. Y. Li, and C. Q. Jin, Solid State Commun. **148**, 538 (2008).
[8] J. H. Tapp, Z. Tang, B. Lv, K. Sasmal, B. Lorenz, P. C. W. Chu, and A. M. Guloy, Phys. Rev. B **78**, 060505(R) (2008).
[9] M. J. Pitcher, D. R. Parker, P. Adamson, S. J. C. Herkelrath, A. T. Boothroyd, R. M. Ibberson, M. Brunelli, and S. J. Clarke, Chem. Commun. 5918 (2008).

[10]F. C. Hsu, J. Y. Luo, K. W. Yeh, T. K. Chen, T. W. Huang, P. M. Wu, Y. C. Lee, Y. L. Huang, Y. Y. Chu, D. C. Yan, and M. K. Wu, Proc. Natl. Acad. Sci. **105**, 14262 (2008).
[11]T. Klimczuk, T. M. McQueen, A. J. Williams, Q. Huang, F. Ronning, E. D. Bauer, J. D. Thompson, M. A. Green, and R. J. Cava, Phys. Rev. B **79**, 012505 (2009).
[12]H. Ogino, Y. Matsumura, Y. Katsura, K. Ushiyama, S. Horii, K. Kishio, and J. Shimoyama, Supercond. Sci. Technol. **22**, 075008 (2009).
[13]X. Zhu, F. Han, G. Mu, P. Cheng, B. Shen, B. Zeng, and H. H. Wen, Phys. Rev. B **79**, 220512(R) (2009).
[14]J. Guo, S. Jin, G. Wang, S. Wang, K. Zhu, T. Zhou, M. He, and X. Chen, Phys. Rev. B **82**, 180520(R) (2010).
[15]E. D. Bauer, F. Ronning, B. L. Scott, and J. D. Thompson, Phys. Rev. B **78**, 172504 (2008).
[16]N. Berry, C. Capan, G. Seyfarth, A. D. Bianchi, J. Ziller, and Z. Fisk, Phys. Rev. B **79**, 180502 (2009).
[17]F. Ronning, E. D. Bauer, T. Park, S. H. Baek, H. Sakai, and J. D. Thompson, Phys. Rev. B **79**, 134507 (2009).
[18]D. Hirai, T. Takayama, D. Hashizume, R. Higashinaka, A. Yamamoto, A. K. Hiroko, and H. Takagi, Physica C **470**, S296 (2010).
[19]H. Fujii and A. Sato, Phys. Rev. B **79**, 224522 (2009).
[20]K. Kudo, Y. Nishikubo, and M. Nohara, J. Phys. Soc. Jpn. **79**, 123710 (2010).
[21]J. R. Neilson, T. M. McQueen, A. Llobet, J. J. Wen, and M. R. Suchomel, Phys. Rev. B **87**, 045124 (2013).
[22]H. Mizoguchi, S. Matsuishi, M. Hirano, M. Tachibana, E. Takayama-Muromachi, H. Kawaji, and H. Hosono, Phys. Rev. Lett. **106**, 057002 (2011).
[23]X. Lin, W. E. Straszheim, S. L. Bud'ko, and P. C. Canfield, J. Alloys Compd. **554**, 304 (2013).
[24]A. Thamizhavel, A. Galatanu, E. Yamamoto, T. Okubo, M. Yamada, K. Tabata, T. C. Kobayashi, N. Nakamura, K. Sugiyama, K. Kindo, T. Takeuchi, R. Settai, and Y. Onuki, J. Phys. Soc. Jpn. **72**, 2632 (2003).
[25]G. M. Sheldrick, Acta Cryst. A **64**, 112 (2008).
[26]A. C. Larson, R. B. Von Dreele, General Structure Analysis System (GSAS), Los Alamos National Laboratory Report LAUR 86–748 (2000).
[27]C. Malliakas, S. J. L. Billinge, H. J. Kim, and M. G. Kanatzidis, J. Am. Chem. Soc. **127**, 6510 (2005).
[28]M. A. Zhuravleva, M. Evain, V. Petricek, and M. G. Kanatzidis, J. Am. Chem. Soc. **129**, 3082 (2007).
[29]C. D. Malliakas and M. G. Kanatzidis, J. Am. Chem. Soc. **129**, 10675 (2007).
[30]C. D. Malliakas, M. Iavarone, J. Fedor, and M. G. Kanatzidis, J. Am. Chem. Soc. **130**, 3310 (2008).
[31]D. L. Gray, M. C. Francisco, and M. G. Kanatzidis, Inorg. Chem. **47**, 7243 (2008).
[32]C. D. Malliakas and M. G. Kanatzidis, J. Am. Chem. Soc. **131**, 6896 (2009).
[33]G. Grüner, Rev. Mod. Phys. **60**, 1129 (1988).
[34]M. D. Johannes and I. I. Mazin, Phys. Rev. B **77**, 165135 (2008).
[35]J. Laverock, S. B. Dugdale, Zs. Major, M. A. Alam, N. Ru, I. R. Fisher, G. Santi, and E. Bruno, Phys. Rev. B **71**, 085114 (2005).
[36]P. W. Anderson, J. Phys. Chem. Solids **11**, 26 (1959).
[37]M. H. Jung, A. H. Lacerda, and T. Takabatake, Phys. Rev. B **65**, 132405 (2002).
[38]V. L. Ginzburg and L. D. Landau, Zh. Eksp. Teor. Fiz. **20**, 1064 (1950).
[39]D. Singh, *Planewaves, Pseudopotentials, and the LAPW method* (Kluwer, Boston, 1994).
[40]W. Kohn and L. J. Sham, Phys. Rev. **140**, A1133 (1965).
[41]P. Hohenberg and W. Kohn, Phys. Rev. **136**, B864 (1964).
[42]J. P. Perdew, K. Burke, and M. Ernzerhof, Phys. Rev. Lett. **77**, 3865 (1996).
[43]D. D. Koelling and B. N. Harmon, J. Phys. C: Solid State Phys. **10**, 3107 (1977).
[44]K. Schwarz, P. Blaha, and G. K. H. Madsen, Comput. Phys. Commun. **147**, 71 (2002).
[45]J. Park, G. Lee, F. Wolff-Fabris, Y. Y. Koh, M. J. Eom, Y. K. Kim, M. A. Farhan, Y. J. Jo, C. Kim, J. H. Shim, and J. S. Kim, Phys. Rev. Lett. **107**, 126402 (2011).
[46]I. I. Mazin, D. J. Singh, M. D. Johannes, and M. H. Du, Phys. Rev. Lett. **101**, 057003 (2008).
[47]A. D. Christianson, E. A. Goremychkin, R. Osborn, S. Rosenkranz, M. D. Lumsden, C. D. Malliakas, I. S. Todorov, H. Claus, D. Y. Chung, M. G. Kanatzidis, R. I. Bewley, and T. Guidi, Nature (London) **456**, 930 (2008).
[48]M. G. Holder, A. Jesche, P. Lombardo, R. Hayn, D. V. Vyalikh, S. Danzenbacher, K. Kummer, C. Krellner, C. Geibel, Y. Kucherenko, T. K. Kim, R. Follath, S. L. Molodtsov, and C. Laubschat, Phys. Rev. Lett. **104**, 096402 (2010).
[49]Y. He, T. Wu, G. Wu, Q. J. Zheng, Y. Z. Liu, H. Chen, J. J. Ying, R. H. Liu, X. F. Wang, Y. L. Xie, Y. J. Yan, J. K. Dong, S. Y. Li, and X. H. Chen, J. Phys.: Condens. Matter **22**, 235701 (2010).
[50]J. Paglione and R. L. Greene, Nat. Phys. **6**, 645 (2010).
[51]K. Terashima, Y. Sekiba, J. H. Bowen, K. Nakayama, T. Kawahara, T. Sato, P. Richard, Y. M. Xu, L. J. Li, L. G. H. Cao, Z. A. Xu, H. Ding, and T. Takahashi, Proc. Natl. Acad. Sci. USA **106**, 7330 (2009).
[52]T. Sato, K. Nakayama, Y. Sekiba, P. Richard, Y. M. Xu, S. Souma, T. Takahashi, G. F. Chen, J. L. Luo, N. L. Wang, and H. Ding, Phys. Rev. Lett. **103**, 047002 (2009).
[53]L. Fang, H. Q. Luo, P. Cheng, Z. S. Wang, Y. Jia, G. Mu, B. Shen, I. I. Mazin, L. Shan, C. Ren, and H. H. Wen, Phys. Rev. B **80**, 140508(R) (2009).